Time-Domain Evaluation of Acoustic Liner Impedance from LDV Measurements

Time-Domain Evaluation of Acoustic Liner Impedance from LDV Measurements

Rémi Roncen*
DMPE, ONERA, Université de Toulouse, 31000, Toulouse, France

Ludovic Ambrosiani†
DMPE, ONERA, Université de Toulouse, 31000, Toulouse, France
Politecnico di Torino, Corso Duca degli Abruzzi 24, 10129, Torino, Italy

Estelle Piot‡ & Fabien Mery§
DMPE, ONERA, Université de Toulouse, 31000, Toulouse, France

Francesco Avallone¶
Politecnico di Torino, Corso Duca degli Abruzzi 24, 10129, Torino, Italy

Acoustic liners are passive sound absorbing materials ubiquitous to many domains of engineering, and are typically characterized by a quantity called impedance. When a liner is subject to a strong sound pressure level or in the presence of a shear grazing flow, the impedance changes due to nonlinear effects. The measurement of an impedance is often performed through inverse methods that rely on the effect of the impedance onto some other measurable quantities, such as the acoustic pressure or velocity above the sample. In the presence of such nonlinear behaviors in the liner, a time-domain approach could bring additional understanding into the complex intricacies of flow and noise interactions in the vicinity of the liner. One such approach is developed in the present work, where laser Doppler velocimetry measurements capable of capturing both the turbulence flow and acoustic fields above the liner are used in conjunction with a time-domain impedance model that does not rely on a wave propagation model to evaluate the effective impedance of the liner.

I. Nomenclature

Z, Y, R	=	normalized impedance, normalized admittance, reflection coefficient
$\tilde{r}, \tilde{\chi}$	=	resistance, reactance
$\mathcal{R}$	=	impulse response of the reflection coefficient
ρ_f, c_f	=	density, speed of sound
$\tilde{p}, \tilde{v}_n$	=	acoustic pressure, normal acoustic velocity
M_b	=	bulk Mach number
f, ω	=	frequency, angular frequency
$\mathcal{F}$	=	fast Fourier transform operator
S_h, S_t	=	Shear number, Strouhal number
$k_{\text{Guess}}, k_1, k_2$	=	parameters of the Guess model for flow effects
DIR-TDIBC	=	dynamic impulse response time domain impedance boundary condition

*Research Scientist, Multi-Physics Department for Energetics (DMPE), remi.roncen@onera.fr.
†PhD student, Multi-Physics Department for Energetics (DMPE) & Department of Mechanical and Aerospace Engineering (DIMEAS), ludovic.ambrosiani@onera.fr.
‡Research Scientist, Multi-Physics Department for Energetics (DMPE), estelle.piot@onera.fr.
§Research Scientist, Multi-Physics Department for Energetics (DMPE), fabien.mery@onera.fr.
¶Professor, Department of Mechanical and Aerospace Engineering (DIMEAS), francesco.avallone@polito.it.

II. Introduction

Aeroacoustic liners are widely used as passive noise control devices [1], typically consisting of perforated face sheets backed by cavities. Their performance is commonly described in the frequency domain by the acoustic impedance [2], which quantifies the liner's ability to dissipate acoustic energy in a given system. However, impedance is not a fixed property: it varies significantly with operating conditions, most notably under high sound pressure levels (SPL) or when exposed to a shear grazing flow. In particular, vortex shedding at liner perforations can generate nonlinearities at SPLs far below those required for global nonlinear wave propagation [3–6]. These external dependencies motivate continued efforts to reliably determine impedance in realistic flow and acoustic environments.

Direct measurement of impedance is generally not possible in the presence of flow, except with the intrusive and somehow tricky in-situ method [7, 8]. Instead, researchers rely on indirect approaches known as impedance eduction. These methods combine experimental measurements—typically acoustic pressures or velocity fields in flow ducts—with wave propagation models, and determine the impedance that best reproduces the observed data. Most eduction techniques are frequency-domain and linear, solving harmonic propagation problems given mean flow properties and an impedance boundary condition. Optimization is then used to identify the impedance that minimizes the discrepancy between experiment and model.

The pioneering observations of Renoux and Aurégan [9] revealed that impedance inferred from upstream versus downstream wave propagation was not identical, challenging the long-held assumption that impedance is an intrinsic material property. This triggered a broad research effort into whether impedance alone suffices to capture the complex physics of liner-flow interactions.

A key drawback of eduction strategies is that any deficiency in the propagation model is implicitly absorbed into the retrieved impedance. As a result, educed impedance can depend not only on the duct geometry or experimental method but also on the direction of acoustic waves relative to the mean flow, depending on the method used [10]. However, due to the tight coupling between the wave propagation modeling and the educed impedance, it has so far not been possible to sort out the upstream-downstream mismatch in terms of wave propagation modeling bias and genuine physical effects changing the impedance, such as a momentum transfer [11]. Weng et al. [12] verified that the mismatch was not caused by neglecting viscosity in the wave propagation solvers used for eduction, while Roncen et al. [13, § 3.2] demonstrated that nonlinear effects on the liner can lead to a spatially varying impedance that differs depending on the excitation direction. Nevertheless, the upstream–downstream mismatch has also been observed in contexts where nonlinear liner effects can be neglected, indicating that the full picture remains unresolved. Recently, Quintinio et al. [14] showed that the influence of the flow profile—and in particular that of the boundary-layer displacement thickness—correlated strongly with the differences in educed impedance observed across different test benches. This, in turn, suggests that if the propagation direction of the acoustic wave were to modify the displacement thickness, a direct link could exist between the educed impedance and the relative direction of the wave with respect to the flow.

More recently, it has been suggested that part of the apparent flow dependence of impedance may stem from turbulence-induced noise, via the same nonlinear effects attributed to high SPL [15]. These observations, while sparse, underlined the challenge of disentangling flow from acoustics in traditional eduction frameworks, and showed the interest of considering a fully time-domain approach.

The objective of the present work is to propose an alternative impedance evaluation method that suppresses reliance on wave propagation modeling. The approach exploits laser Doppler velocimetry (LDV) measurements taken directly above the liner and uses the time domain framework developped in Ref. [15, 16] to educe the nonlinear correction of classical impedance models (see Boden's recent review [17]). While this method relies on some assumptions coming from semi-empirical impedance models, it provides impedance estimates that are independent of propagation models and thus offer new insights into the role of flow-induced changes in impedance. In particular, by comparing upstream and downstream loudspeaker configurations, we test whether the observed impedance mismatch is an artifact of propagation modeling or a genuine physical effect.

The theoretical background required for the analysis is introduced in Sec. III, the experimental setup is presented in Sec. IV, and the new methodology is introduced in Sec. V.

III. Theoretical background

This section introduces the theoretical background of liner impedance modeling. Section III.A presents the classical frequency-domain formulation of a single degree of freedom (SDoF) liner. Sections III.B and III.C then discuss the influence of nonlinear and flow effects on impedance. Finally, Section III.D addresses the conversion from frequency to time domain.

A. Acoustic liner impedance

The normalized surface impedance, denoted by Z in the frequency domain, is defined as the ratio of acoustic pressure $\tilde{p}$ to the normal acoustic particle velocity $\tilde{v}_n$ at the liner surface, scaled by the characteristic impedance of the ambient medium, $\rho_f c_f$, where ρ_f is the fluid density and c_f the speed of sound. It is commonly expressed in terms of its real and imaginary parts—resistance $\tilde{r}$ and reactance $\tilde{\chi}$—as

$$Z(\omega) = \frac{\tilde{p}(\omega)}{\rho_f c_f \tilde{v}_n(\omega)} = \tilde{r}(\omega) + \mathrm{j}\tilde{\chi}(\omega), \tag{1}$$

where $\omega = 2\pi f$ is the angular frequency in rad/s, with f the frequency in Hz and j the imaginary unit. It should be emphasized that $\tilde{p}$ and $\tilde{v}_n$ are typically interpreted as homogenized quantities, such that the fine-scale velocity variations within the perforations are not explicitly resolved. Instead, the liner surface is treated as acoustically smooth, and the impedance represents an effective boundary condition, widely used in aeroacoustic numerical solvers.

Two limiting cases illustrate the meaning of impedance: for a perfectly rigid wall, the resistance tends to infinity, whereas for a pressure-release boundary it vanishes. For practical liners comprising cavities, perforations, or other microstructures, the situation is more complex. Interactions between waves and walls generate oscillo-diffusive processes that yield a frequency-dependent impedance. The reactance term, in particular, reflects the phase shifts introduced by waves oscillating within the liner cavities. At certain frequencies, the reactance crosses zero, corresponding to specific constructive or destructive superpositions of incident and reflected waves. In the constructive case, the normal velocity at the perforated face is amplified, which enhances dissipation—a condition known as *resonance*. In contrast, destructive superposition of waves suppresses velocity and leads to reduced dissipation, referred to as *anti-resonance*.

Complex liners are often represented in the frequency domain as assemblies of elementary units using transfer matrix methods [18, Chap. 11]. For clarity, however, a more compact SDoF formulation is adopted in this work, where only one perforated plate and one cavity are considered. Specifically, the normalized impedance of an SDoF liner is expressed following the approach of Atalla and Sgard [19, Eq. 8], with the cavity wavenumber $\tilde{k}_c$ determined using Bruneau's formulation [20, § 3.7]:

$$\begin{aligned}
Z_0(\omega) &= \frac{R_s}{\rho_f c_f \phi_p}\left(\frac{2L_p}{r_p} + 4\frac{\epsilon_e}{r_p}\right)\frac{(1+\mathrm{j})\sqrt{2}}{2} \\
&\quad + \frac{(2\epsilon_e + L_p)}{c_f \phi_p}\mathrm{j}\omega + \frac{1}{\phi_c}\coth\left(\mathrm{j}\tilde{k}_c H_c\right) && \text{(2a)} \\
\epsilon_e &= 0.85 r_p\left(1 - 1.14\sqrt{\phi_p}\right), \quad \text{Correction length} && \text{(2b)} \\
R_s &= \sqrt{\eta\omega\rho_f}, \quad \text{Surface resistance} && \text{(2c)} \\
\mathrm{j}\tilde{k}_c &= \frac{\mathrm{j}\omega}{c_f}\left[\frac{1 + (\gamma-1)\,\Phi(k_\kappa r_c)}{1 - \Phi(k_\nu r_c)}\right]^{1/2}, \quad \text{Cavity wavenumber} && \text{(2d)} \\
\Phi(s) &= \frac{2}{s}\frac{I_1}{I_2}(s). && \text{(2e)}
\end{aligned}$$

Here, an $e^{+\mathrm{j}\omega t}$ convention is assumed, and the formulation is valid for $\omega > 0$. The symbols L_p, ϕ_p, and r_p denote, respectively, the thickness, porosity, and hole radius of the perforated plate, while L_c, ϕ_c, and r_c describe the cavity geometry. I_n are modified Bessel functions of the first kind of order n, with $k_\nu = \sqrt{\mathrm{j}\omega/\nu}$ and $k_\kappa = \sqrt{\mathrm{j}\omega/\kappa}$. The ambient fluid is characterized by the speed of sound c_f, density ρ_f, heat capacity ratio γ, dynamic viscosity η, kinematic viscosity ν, and thermal conductivity κ.

B. Nonlinear effects

Although impedance is formally a concept tied to linear systems, in practice it is often extended to describe nonlinear behavior in the frequency domain when harmonic excitation is considered. While this extension is not strictly rigorous, it has proven effective for characterizing liner performance at high SPL.

Most nonlinear impedance models [3, 4, 17, 21–23] adopt an additive formulation in which the total impedance is expressed as

$$Z_{\mathrm{tot}}(\omega, \tilde{v}_n(\omega)) = Z_0(\omega) + \mathcal{G}_{\mathrm{NL}}(\omega, \tilde{v}_n(\omega)), \tag{3}$$

where $Z_0(\omega)$ is the baseline linear impedance, and $\mathcal{G}_{\mathrm{NL}}$ is a nonlinear contribution that depends on frequency, perforation geometry, plate porosity, and the normal velocity $\tilde{v}_n(\omega)$ at the liner surface.

In this study, the nonlinear correction $\mathcal{G}_{\mathrm{NL}}$ is split into real and imaginary parts using models recommended in Bodén's recent review [17]. The real component is estimated using Temiz et al.'s formulation [23, Eq. 13], while the imaginary part is modeled with Shah's correction [24, Eq. 14]. For reference, these *empirical* models are provided here for $\omega > 0$:

$$\mathrm{Re}\left(\mathcal{G}_{\mathrm{NL}}\right) = \frac{\sqrt{2}\,|\tilde{v}_n|}{\phi_p^2 c_f}\frac{1}{2C_{\mathrm{vc}}^2}\frac{1}{1+2S_t\cdot\left(1+0.06\mathrm{e}^{\frac{3.74}{S_h}}\right)}, \tag{4a}$$

and

$$\mathrm{Im}\left(\mathcal{G}_{\mathrm{NL}}\right) = \frac{k_f r_p}{\phi_p}\left[-\left(0.6+1.6{S_h}^{-1}+0.015S_h\right)\left(1-\frac{1}{1+0.013{S_t}^{-2.5}{S_h}^2}\right)\right], \tag{4b}$$

where $C_{\mathrm{vc}} = 0.8$ is the vena contracta coefficient, S_h is the Shear wave number, S_t the Strouhal number based on the particle velocity root mean square (rms) inside the perforation $u_p(\omega) = |\tilde{v}_n(\omega)|/\phi_p$:

$$S_h = r_p\sqrt{\frac{\omega}{\nu}}, \tag{5a}$$

$$S_t = \frac{2\omega r_p}{\sqrt{2}u_p(\omega)}. \tag{5b}$$

Note that no adjustments to the correction length in Eq. 2 for nonlinear effects have been considered in this work, in order to preserve the general additive approach outlined in Eq. 3.

C. Flow effects

Typically, in the presence of a shear grazing flow, an additional contribution to the impedance is added, as

$$Z_{\mathrm{tot}}\left(\omega,\tilde{v}_n(\omega)\right) \leftarrow Z_{\mathrm{tot}}\left(\omega,\tilde{v}_n(\omega)\right) + \mathcal{G}_{\mathrm{flow}}\left(\mathbf{U_0}\right), \tag{6}$$

where $\mathcal{G}_{\mathrm{flow}}(\mathbf{U_0})$ is usually a real function of the liner's flow-facing porosity and of the flow profile $\mathbf{U_0}$. A common simplification is to consider the Guess model [21], which was obtained by fitting the experimental data of Dean & Feder [25], as

$$\mathcal{G}_{\mathrm{flow}}\left(\mathbf{U_0}\right) = \frac{1-\phi^2}{\phi}k_{\mathrm{G}}M_{\mathrm{b}}, \tag{7}$$

where $k_{\mathrm{G}} \approx 0.3$ and M_{b} is the bulk Mach number. It is important to note that the data of Dean & Feder were obtained using a specific configuration in which a loudspeaker was placed behind the sample exposed to flow. Consequently, the Guess model derived from these measurements does not incorporate upstream–downstream asymmetry [25, Fig. 5].

In the remainder of this work, impedance evaluation within the time-domain framework does not include flow contributions through the Guess model or related formulations of Eq. 6. Instead, only the linear and nonlinear terms of Eq. 3 are retained, with the turbulence induced noise signature entering the effective impedance indirectly via these nonlinear effects driven by the value of $\tilde{v}_n$. We hypothesize, following a previous initial exploration [15, Sec. 5], that the empirical fits proposed by Guess and subsequent authors are, at least in part, influenced by this mechanism—that is, by flow noise being redistributed into the impedance through nonlinear interactions. Although flow noise predominantly lies at frequencies much lower than those typically investigated in duct acoustics, nonlinear coupling can shift its impact to higher frequencies. Testing this hypothesis is therefore one of the central objectives of the present paper.

It is worth noting that the numerical method employed throughout this work is formulated in terms of the liner's reflection coefficient. The reflection coefficient, sometimes referred to as the scattering operator R, is bounded within the complex unit circle, which makes it particularly convenient and numerically stable for simulation purposes, i.e., one can write a solver whose CFL is reflection coefficient independent [26, §3.3; 27, §2.3; 28, §5.3]. Moreover, R is bijectively related to the normalized impedance through the relation

$$R\left(\omega,\tilde{v}_n(\omega)\right) = \frac{Z_{\mathrm{tot}}\left(\omega,\tilde{v}_n(\omega)\right)-1}{\tilde{Z}_{\mathrm{tot}}\left(\omega,\tilde{v}_n(\omega)\right)+1}. \tag{8}$$

In practice, however, results are reported in terms of impedance, as this representation is the most commonly used and readily interpreted within the liner community.

D. The impulse response approach to TDIBC

To evaluate the time-domain response of a liner, the frequency-domain reflection coefficient must first be recast as a time-domain operator. The liner response to an arbitrary incident wave can then be obtained via convolution with this operator. A practical way to achieve this—one time step at a time—is through the impulse response, i.e., the system's output to a Dirac pulse. In discrete form, the reflection coefficient can thus be represented as a finite-length impulse response array $\mathcal{R}$, evaluated as

$$\mathcal{R} = \mathcal{F}^{-1}\{R\left(\omega, \tilde{v}_n\left(\omega\right)\right)\} \tag{9}$$

where $\mathcal{F}^{-1}$ is the inverse Fourier transform operator.

Each time step of the incident wave is processed by multiplying its amplitude with this impulse response, and the resulting contributions are accumulated in a memory array that stores both present and future terms of the outgoing wave. Using a simple "add-and-shift" procedure, one updates the memory at each time step: the first element, corresponding to the outgoing wave at the current step, is released, and the array is shifted by one. As a result, the memory cost of the method is fixed at the initialization stage.

When nonlinear effects are relevant, the impulse response depends also on the instantaneous acoustic velocity at the liner surface, which is a function of both incoming and reflected waves. In this case, the velocity must be evaluated at each time step so that the impulse response can be updated accordingly.

This approach, known as the dynamic impulse-response time-domain boundary condition (DIR-TDIBC), has been shown to accurately capture the nonlinear impedance of acoustic liners under high-SPL conditions in impedance tubes [15, 16]. It was also shown in Ref. [15] that it is the instantaneous velocity that needs to be considered in this type of problem, and not the root mean square one, especially for complex signals.

IV. Laser doppler velocimetry experiment in the B2A

This section introduces the particular experimental setup used at ONERA for the liner characterization under shear grazing flow conditions. Section IV.A presents the B2A wind tunnel facility, Sec. IV.B on the LDV setup, and Sec. IV.C introduces the liner sample used in this work.

A. The B2A

The ONERA B2A facility consists of a 4-m-long stainless-steel duct with a square cross-section of 50×50 mm. The 0.2-m long test section is equipped with silica windows for optical access, and the duct termination features a quasi-anechoic outlet, yielding an upstream reflection coefficient below 0.2 for frequencies above 500 Hz. The facility can generate fully developed turbulent flows with bulk Mach numbers up to $M_b = 0.6$, where the turbulence intensity in the test-section centerline is on the order of a few percent. A schematic of the B2A duct is shown in Fig. 1, with flow propagating from left to right.

Two acoustic drivers located upstream or downstream of the test section can produce multitone signals of up to 150 dB over the frequency range 0.3–3.5 kHz. The test liner occupies a 150-mm-long segment of the lower duct wall.

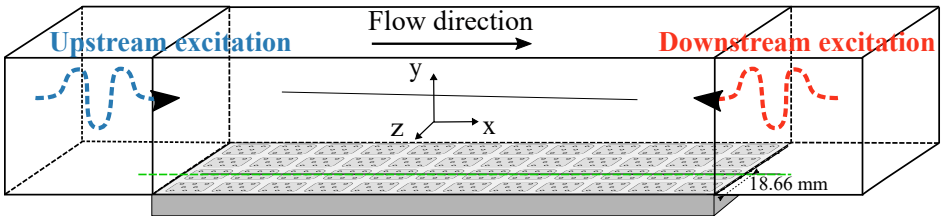

Fig. 1 Schematics of the LDV measurement. Upstream an downstream excitation are never on simultaneously.

B. LDV setup

A two-component fringe-mode LDV system enables measurement of both axial and vertical velocity components across nearly the entire volume of the test section. The emitting optics generate an elliptical measurement volume with a minor axis as small as 70 μm. Flow is seeded with amorphous silica particles, chosen for their low tendency to deposit on optical windows. Because particles arrive randomly in the measurement volume, the LDV signal is unevenly

sampled; a reconstruction algorithm is used to resample the raw data at a uniform rate by the use of a linear interpolation in time. Signal processing is performed using python scripts. Each velocity component is measured at a minimum rate of $f_m \approx 15{,}000$ samples per second, with more than 250,000 total samples acquired per experiment.

Experiments were conducted under standard atmospheric conditions, with the flow temperature maintained at ambient $T_0 \approx 20\ ^\circ$C, with maximum fluctuations of 1 $^\circ$C, corresponding to a sound speed of $c_0 \approx 343$ m/s. The mass flow rate was maintained constant at 300g/s all along the experiments, corresponding to a bulk Mach number $M_b = 0.3$.

The resulting LDV dataset comprises over 120 spatial measurement points. The system provides 2-D velocity fields in the x line at $y = 1$mm from the liner surface and $z = 6.34$mm away from the center of the sample, centered in the middle of a line of cavities, as shown as a green dashed line in Fig. 1 and Fig. 2. Only the streamwise and vertical (normal to the liner) components are measured.

C. Liner sample

The acoustic liner used for this study is an SDoF liner made of a perforated plate over squared cavities based on a geometry shared between multiple facilities [29]. Each cavity is covered by a thin plate of 0.635mm with 8 orifices of diameter $d_p = 2r_p = 0.99$ mm for a total porosity of $\phi_p = 0.0395$. The cavity is $H_c = 38.1$ mm deep and $D = 0.99$mm large. A top view sketch is given in Fig. 2.

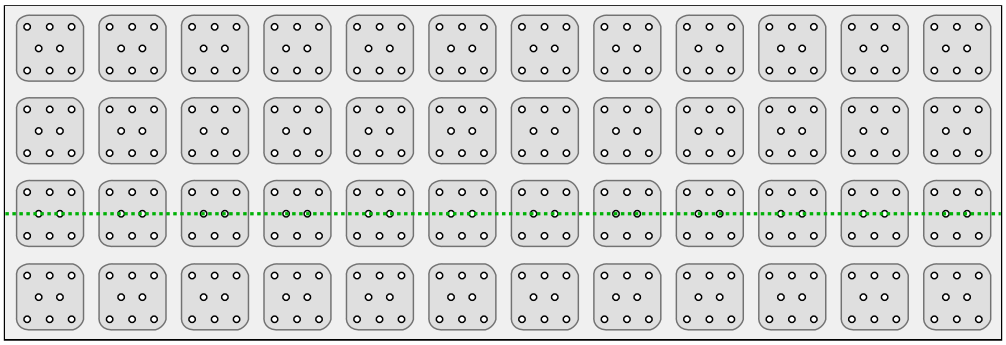

Fig. 2 Top view sketch of the liner SDoF sample. The green line represent the position of the measurement line.

D. An important modeling choice

A notable characteristic of the tested liner sample warrants attention. The sample consists of N elementary cells separated by relatively thick walls, which collectively occupy approximately 37% of the liner surface area, as illustrated in Fig. 3. Using the notations in the figure, this corresponds to $\Sigma_2/\Sigma_1 = 0.63$.

When the entire cell area (Σ_1) is considered, the global porosity of the liner is $\phi_p = 3.95\%$. Restricting the analysis to only the perforated regions of each cell, i.e., excluding the cavity walls, the effective local porosity based on Σ_2 increases to 6.5%.

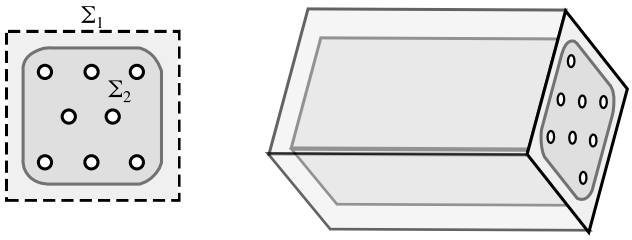

Fig. 3 Top view an side view perspective of a liner cell.

To correctly represent the impedance under this interpretation, the liner can be modeled as a metasurface composed of two distinct cell types: rigid walls in $\Sigma_1 \setminus \Sigma_2$ and single-degree-of-freedom (SDoF) resonators with a porosity of $\phi = 6.5\%$ in Σ_2. This modeling choice has implications for the predicted nonlinear behavior of the liner, since nonlinear effects are directly influenced by the local porosity, see Eqs. 4a and 4b. For the present study, we adopt this interpretation

and will revisit it once additional data becomes available to further validate or challenge this hypothesis. Overall, our choice seems to be aligned with the recent conclusions of Jones et al. [30].

V. Direct impedance evaluation using the DIR-TDIBC

The goal of this section is to see whether, using LDV measurements taken above the liner, the DIR-TDIBC can be used to retrieve an impedance value of the liner. The specific algorithmic method used in this section is introduced in Sec. V.A, and impedance eduction results are shown in Sec. V.B.

A. Procedure of the method

The objective of the proposed method is to generate, from a prescribed incident wave, a reflected wave that captures the nonlinear behavior of the aeroacoustic liner. To this end, the DIR-TDIBC method is employed throughout, as it has demonstrated strong performance in modeling such phenomena. A key limitation, however, is that the incident wave at the liner surface is not directly measurable. Instead, only the total velocity field immediately above the liner is accessible.

The LDV system provides measurements of the wall-normal velocity slightly above the liner surface. This signal comprises several contributions: the mean flow component v_0, turbulent fluctuations $\tilde{v}$, and acoustic perturbations v', such that

$$v_{\text{tot}}(t) = v_0 + \tilde{v}(t) + v'(t) . \tag{10}$$

In previous studies by the present authors, as well as in most impedance eduction approaches based on LDV measurements, the acoustic component v' was isolated from the total signal by a turbulence rejection technique based on cross-correlation using the loudspeaker excitation as a reference. In the present work, this separation step is no longer required. On the contrary, it is hypothesized that both turbulence-induced fluctuations and the mean flow contribution can be incorporated into the nonlinear impedance model in a manner analogous to acoustic perturbations. Consequently, the measured total wall-normal velocity v_{tot} is directly used within the DIR-TDIBC framework, effectively "setting" the nonlinearity.

In practice, at each time step, the impulse response defined in Eq. 9 is recomputed using v_{tot} in place of $\tilde{v}_n(\omega)$.

When an acoustic excitation is present during the experiment, the input signal to the DIR-TDIBC can be defined as an acoustic wave matching the frequency content of the source (e.g., a sine wave). It is important to note, however, that this imposed wave does not directly govern the nonlinear response of the liner. Rather, the nonlinearity is driven by the total velocity v_{tot}, which is used during the DIR-TDIBC updates.

B. Results at Mach 0.3 with an acoustic excitation

Measurements were performed during an LDV experiment at Mach 0.3 with an acoustic excitation at 1500 Hz and 145dB (incident SPL). The experiment was performed with both loudspeakers being either upstream or downstream of the liner section. The methodology described in Sec. V.A is performed on each of the ≈ 120 LDV measurement points located on a line 1mm above the liner, see Fig. 1.

The extracted normal velocity signals immediately upstream and downstream of the liner, for the configuration where the loudspeakers are located upstream, are shown in both the time and frequency domains in Fig. 4, highlighting the relative amplitude of flow noise compared to the acoustic excitation, as well as their frequency separation: flow noise is predominantly concentrated at very low frequencies. As expected, the tonal component associated to the acoustic excitation is strongly reduced downstream of the lined region. In both cases, although the acoustic excitation is clearly visible in the frequency spectrum, the time-domain signal remains highly irregular. At 145 dB and for an impedance of 1, the velocity induced by the acoustic excitation is below 1 m/s, which is small compared to the hydrodynamic fluctuations shown in Fig. 4.

To obtain a single impedance value from all the LDV measurement locations, the admittance Y (inverse of the impedance Z) was averaged. This is akin to considering the material as a parallel assembly of non-communicating cells having each their own impedance values. Once the mean admittance is calculated, the resulting impedance is considered to be the effective global impedance of the liner, close to what a classical impedance eduction approach would "see". In practice, this averaging has limits, especially as the frequency increases and the homogenization performed becomes less valid.

Impedance results obtained at the excitation frequency, i.e., 1500Hz, are shown at each of the LDV measurement points in Fig. 5. The impedance values share the same order of magnitude, and have an average very close to one another

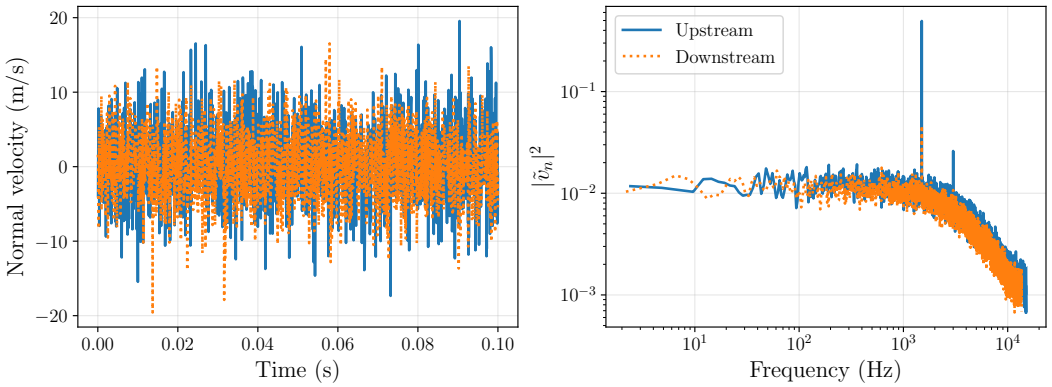

Fig. 4 Normal velocity measured 1 mm above the liner surface, immediately upstream and downstream of the lined wall. Loudspeakers are located upstream. Time-domain signal (left) and corresponding frequency-domain power spectrum (right).

(2.33 − 0.30j and 2.25 − 0.30j for the upstream and downstream cases, respectively), but they demonstrate different trends. Indeed, we initially expected the resistance to decrease along the liner in the direction of wave propagation. Instead, the resistance increases over the liner in the direction of the flow, irrespective of the acoustic source location. This goes directly against our previous work, where we had assumed that the nonlinear behavior of the liner, related to SPL only, would mean a decrease in the resistance over the liner in the direction of the incident wave [13, 31]. This could be related to the turbulence level increasing over the liner, and thus contributing more strongly to the impedance, and to the mean flow effect related to the shear layer development above the liner [32]. In Refs. [13, 31], the Mach number was kept at 0.1 for these tests, which might explain why good agreement was still found with a decreasing impedance: the noise level of the turbulent flow was possibly not high enough to seriously impact the educed impedance. We conclude for now that potential antagonist effects (flow versus acoustics) are present in the upstream case, whereas the effects contribute similarly to a change of resistance in the downstream case.

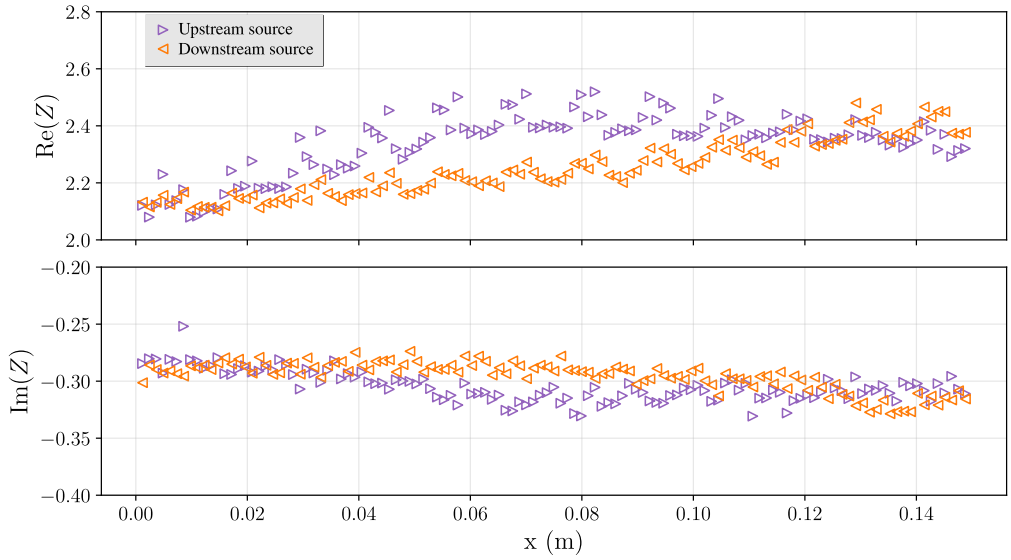

Fig. 5 Comparison of the impedance obtained via TDIBC at 1500Hz, as a function of space. Top: resistance, Bottom: reactance.

C. Usefulness of the educed impedance

To assess the validity of the obtained impedance, its values are reinjected into a linearized Euler equation (LEE) solver, and the resulting wall pressures on the side opposite the liner are compared with experimental measurements. As shown in Fig. 6, the LEE predictions closely match the measured pressures, confirming the physical consistency and reliability of the educed impedances for both upstream and downstream source configurations.

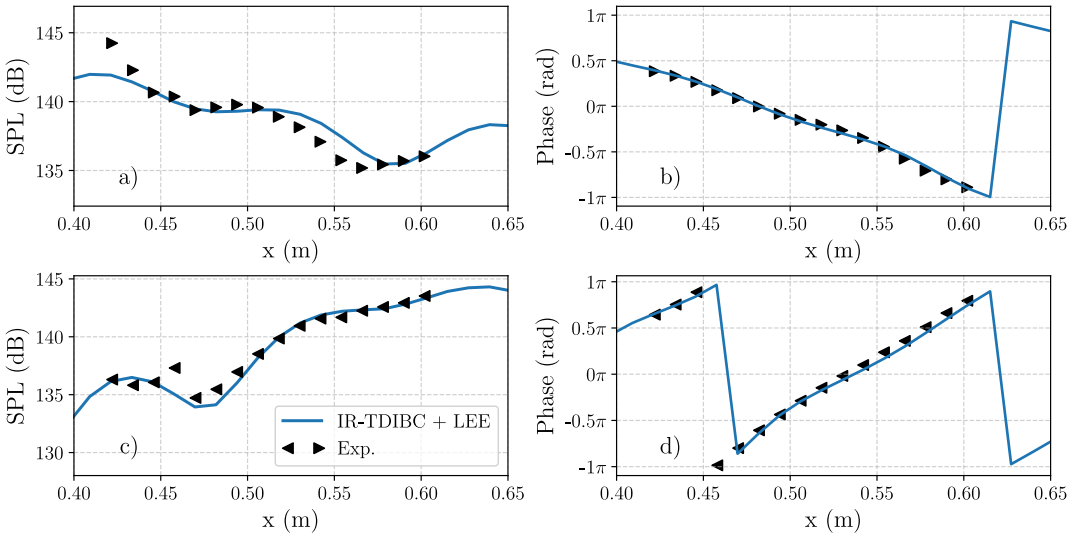

Fig. 6 Comparison of acoustic pressure—(a, c) SPL and (b, d) phase—between experimental microphone measurements in the B2A facility at Mach 0.3 (symbols) and numerical predictions from a 2D-LEE solver (lines), using the impedance stemming from the DIR-TDIBC approach. Top row (a, b) corresponds to upstream source; bottom row (c, d) corresponds to downstream source. Flow goes from left to right, Mach 0.3. Liner located between $x = 0.437$m and $x = 0.587$m.

D. Comparison with direct eduction approach

For comparison with previous DIR-TDIBC results, the microphone pressure data were also analyzed using a classical frequency-domain eduction approach based on the KT algorithm. This method fits a wavenumber to the pressures above the liner and retrieves Z from the wavenumber-impedance relation, assuming a uniform mean flow, as in Ref. [9], where the upstream–downstream impedance mismatch was first identified.

The analysis focuses on Mach 0.3, considering both upstream and downstream excitations. To assess uncertainty, the pressures were perturbed with a standard deviation of 5 Pa in both real and imaginary components. The resulting impedances and SPL fits are shown in Fig. 7. While the measured and modeled pressures agree well, the retrieved impedances differ markedly between upstream ($1.28 + 0.06$j) and downstream ($3.02 - 0.40$j) configurations.

For reference, the DIR-TDIBC impedances for upstream and downstream cases ($2.33 - 0.30$j and $2.25 - 0.30$j, respectively) lie nearly on the line connecting the upstream and downstream KT results, as illustrated in Fig. 7. These results demonstrate that the present method produces a consistent single impedance value regardless of whether the source is upstream or downstream of the liner, while accurately predicting the liner's behavior. If confirmed across additional configurations, this finding would suggest that the previously observed upstream–downstream impedance mismatch arises from an eduction bias rather than a true physical effect.

VI. Impedance prediction using bench flow characteristics

Given the previous tests, it is reasonable to attribute at least part of the flow effect to hydrodynamic perturbations. Potential discrepancies between different test benches may therefore stem from bench-specific characteristics of these fluctuations, such as variations in Reynolds number at a given Mach number, differences in flow straightening techniques or facility test section aspect ratio.

To further explore the potential of the DIR-TDIBC as a tool for impedance prediction with flow, a series of analyses

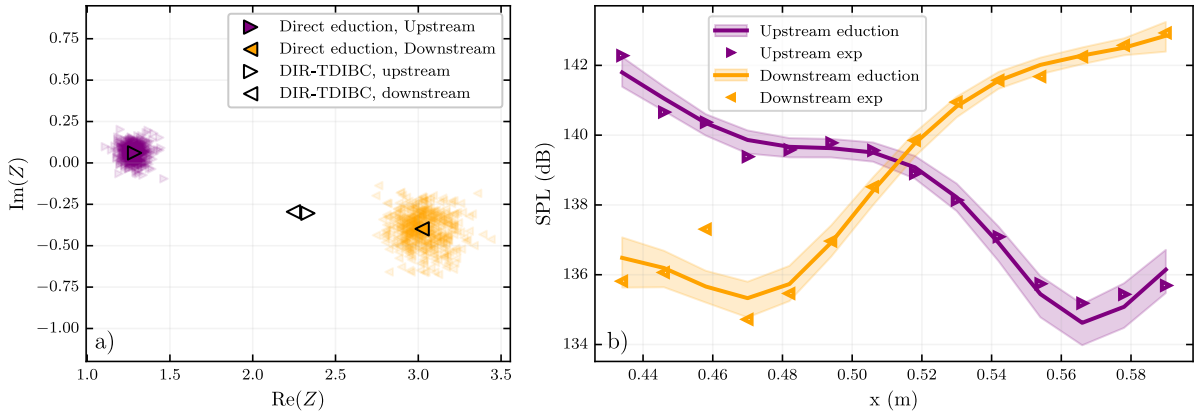

Fig. 7 Results of the direct eduction approach at Mach 0.3 with an excitation frequency of 1500 Hz, based on pressure microphones located on the wall opposite the liner. (a) Impedances in the complex plane for each sample and their mean, as well as the mean impedance obtained via DIR-TDIBC. (b) Corresponding comparison of measured and predicted SPL above the liner. The shaded envelope denotes the minimum and maximum limits across samples. Flow goes from left to right. Liner located between $x = 0.437$m and $x = 0.587$m.

is conducted. LDV measurements were acquired upstream of the liner sample in the absence of acoustic excitation. Measurements were performed at various distances from the wall and for Mach numbers ranging from 0.1 to 0.3.

The wall-normal velocity signals obtained from these measurements can be used to predict the acoustic response of a liner subject to such perturbations, in which only flow-induced noise is present. To extend this approach, we also aim to examine the influence of SPL by imposing a target total SPL on the liner. The objective is to investigate the potential interaction, or rather, competition, between SPL and flow effects. To this end, the DIR-TDIBC methodology described in Sec. V.A is updated in Sec. VI.A, and the results are presented in Sec. VI.B.

A. Updated DIR-TDIBC procedure to impose a total SPL

Given a user-specified total pressure at the liner facesheet, the corresponding acoustic velocity at the target frequency is first calculated using the linear impedance relation in the frequency domain. The total velocity is then updated by adding the fixed flow-induced contribution measured by LDV, $v_{\mathrm{LDV}}(t)$, to a sine wave whose amplitude is determined from the impedance relation. The DIR-TDIBC is then applied to this synthetic signal. This process produces an artificial reflected wave, from which the reflection coefficient—and hence the impedance—can be deduced. The total acoustic velocity is then recalculated from this impedance value, and the procedure is repeated until convergence of the reflection coefficient is achieved, defined here as an absolute change below 10^{-3}.

B. Results

LDV measurements were obtained at Mach 0.1, 0.2 and 0.3 in the B2A, 3mm upstream of the liner, at wall distances ranging from 0.78mm to 1.7mm. The DIR-TDIBC approach was then applied on these signals, super-imposing sine wave contributions whose velocity matched, after the convergence described in Sec. VI.A, a total SPL ranging from 100 to 160dB, at frequencies ranging from 300 to 6000 Hz with 50Hz increments. One of the advantages of the method resides in its capacity to evaluate the impedance at frequencies beyond that of the plane wave limit of the bench.

Additionally, the case Mach 0 is considered by setting the LDV velocity to 0 and performing the same analysis.

Since the LDV signal is long, it is separated in 18-20 segments of 1s each, and the analysis is repeated multiple times, yielding a sense of uncertainty quantification in the results.

The joint effect of the Mach and of the SPL effects is shown in Figs. 8 and 9, where the resistance and reactance obtained are shown, respectively. In this case, the LDV measurements are taken at a wall-normal distance of 1 mm, and the results were found to exhibit only weak sensitivity to this parameter within the range considered.

Focusing on Fig. 8, it is observed that resistance increases with both Mach number and SPL, though the two effects interact in a competitive manner. Near the resonance at 1500 Hz, the resistance increase due to higher SPL is more pronounced at lower Mach numbers. Interestingly, in some extreme cases—particularly for SPLs above 150 dB near resonance (1500 Hz and 5500 Hz)—an increase in Mach number can lead to a reduction in resistance, an effect not

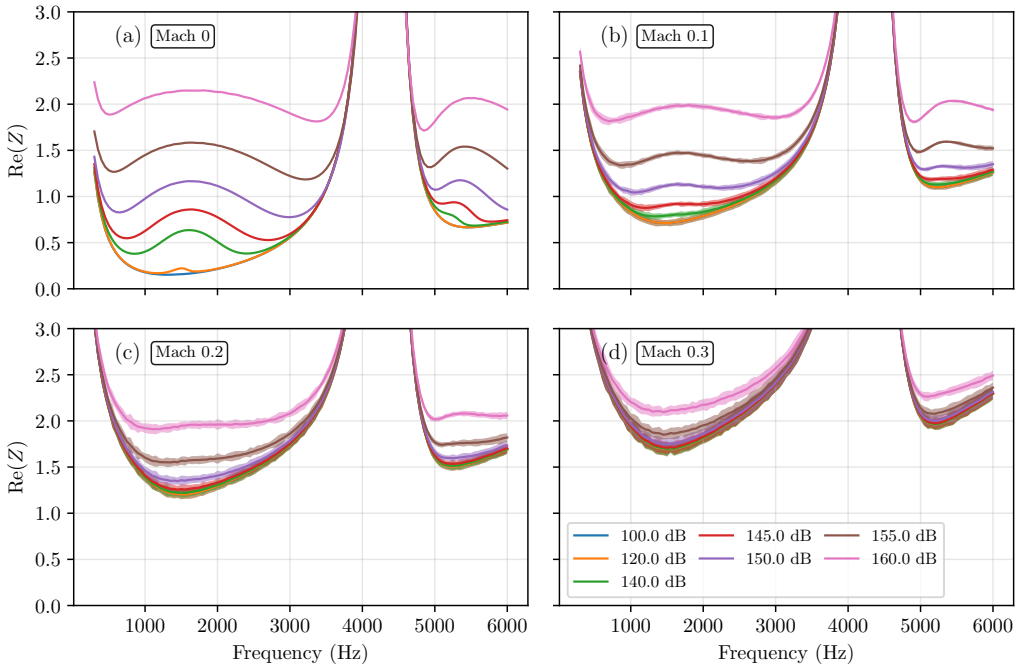

Fig. 8 Comparison of resistance against frequency, for different Mach numbers and total SPL.

anticipated a priori.

The reactance in Fig. 9 exhibits a strong SPL dependence in the absence of flow: near resonance, increasing SPL reduces the reactance, as expected. However, this SPL-induced variation diminishes rapidly with increasing Mach number. Literature suggests that higher Mach numbers should decrease the reactance, but this trend is not captured by the current model. This discrepancy indicates that the flow signature measured by the upstream LDV may be insufficient to reproduce this effect. Previous studies have speculated that at higher Mach numbers, the convective transport of air within the perforations reduces the effective inertial mass, thereby influencing the reactance. The present approach does not account for this phenomenon.

Figure 10 illustrates the increase in resistance as a function of Mach number for various frequencies and SPL levels. The change in resistance relative to the Mach 0 case is denoted as $\Delta \mathrm{R}\,(Z)$. A direct observation from Fig. 10 is that, at high SPL, the influence of the flow is reduced. This behavior is consistent with the flow effects reported by Léon et al. [33]. Interestingly, this effect is less pronounced near the anti-resonance at 4.5 kHz, where the influence of SPL is comparatively smaller. At low frequencies (i.e., 500 Hz), the flow effect appears more pronounced. This may be related to the flow signature, which exhibits greater energy in the low-frequency range (see Fig. 4).

If the preceding results are confirmed and the model validated across all examined regimes, this would suggest that, for certain liners exhibiting nonlinear SPL-dependent behavior, the flow-effect corrections proposed by empirical models (e.g., Guess [21]) may depend not only on Mach number and boundary-layer characteristics but also on frequency and SPL. Focusing on the Guess model, which is expressed as

$$\Delta \mathrm{R}_{\mathrm{Guess}}\,(Z) = k_{\mathrm{Guess}} \frac{1-\phi^2}{\phi} M_{\mathrm{b}}, \tag{11}$$

with $k_{\mathrm{Guess}} = 0.3$ and M_{b} denoting the bulk Mach number, one can recalculate the value of k_{Guess} based on the results in Fig. 10. A strong assumption, which is clearly not supported by the data, is that k_{Guess} depends linearly on Mach number. We therefore propose an extended Guess model of the form

$$\Delta \mathrm{R}_{\mathrm{Guess}}\,(Z) = \frac{1-\phi^2}{\phi}\left(k_1 M_{\mathrm{b}} + k_2 M_{\mathrm{b}}^2\right), \tag{12}$$

where k_1 and k_2 are determined via curve fitting. The resulting values are shown in Fig. 11. For low SPL and especially at low frequencies, k_1 is close to 0.3, consistent with the original Guess model, and decreases as SPL increases. In

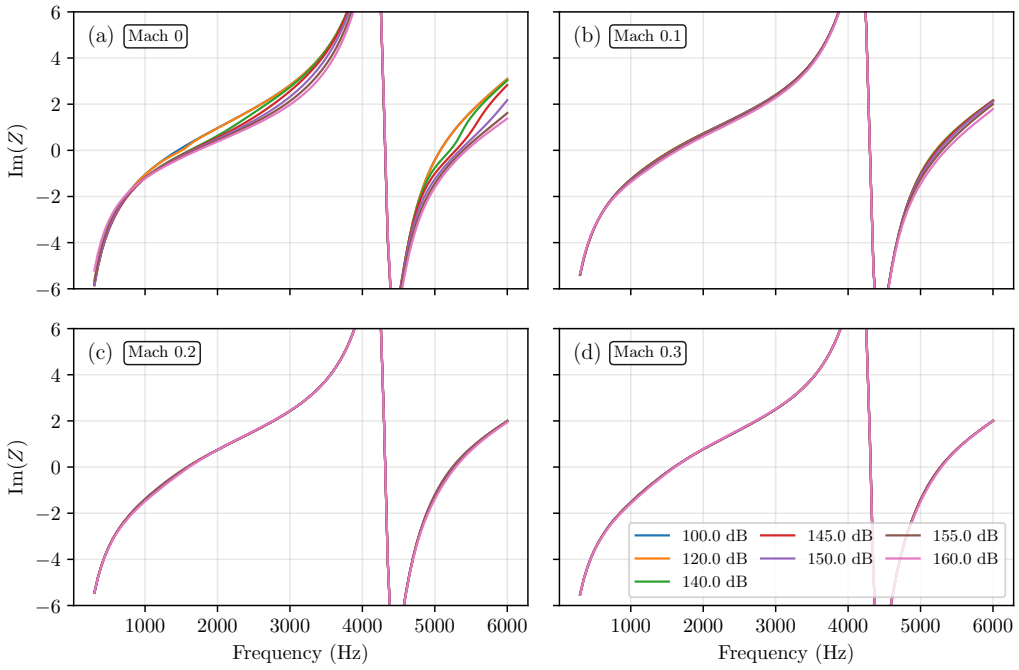

Fig. 9 Comparison of reactance against frequency, for different Mach numbers and total SPL.

contrast, k_2 grows with SPL, highlighting the increasing significance of nonlinear Mach effects at higher SPL levels. As a perspective, it would be valuable to further investigate the obtained parameters to identify relationships among the linear impedance, frequency, SPL, and Mach number.

VII. Conclusion

In this study, the DIR-TDIBC methodology was applied to characterize the impedance of an acoustic liner under combined flow and high-SPL conditions. The approach successfully captures nonlinear effects and provides a single, consistent impedance value regardless of upstream or downstream source positions, overcoming limitations observed with classical eduction methods. Comparisons with experimental pressure measurements and linearized Euler equation simulations confirm the physical validity of the educed impedances. In addition, a spatially-varying impedance can be obtained over the liner, paving the way for improved characterizations that do not rely on wave propagation tools.

The analysis highlights the complex interplay between flow effects—attributed to hydrodynamic fluctuations in the wall-normal velocity—and the total SPL experienced by the perforated liner, affecting both the resistive and reactive components of the impedance. In particular, a competition between flow and SPL effects is demonstrated for a representative liner over Mach numbers ranging from 0 to 0.3 and SPL levels between 100 dB and 160 dB.

An extended Guess model was proposed to account for nonlinear Mach dependencies, indicating that empirical flow corrections may need to incorporate frequency and SPL effects in addition to Mach number. However, no simple trends could be identified for this extended model, highlighting the need for further investigation to enable rapid evaluation of coupled flow–SPL effects in the frequency domain.

In contrast, within a time-domain framework, the DIR-TDIBC approach provides a direct means of capturing these effects without relying on empirical flow-correction models.

Overall, the results demonstrate that DIR-TDIBC, combined with high-resolution LDV measurements, is a robust tool for predicting liner behavior in nonlinear acoustic regimes. Future work could focus on extending the methodology to a broader range of liner configurations and flow conditions. Additionally, performing LDV measurements downstream of the liner and applying the method at this location could yield higher impedance values, as the liner may modify the hydrodynamics of the flow along its surface.

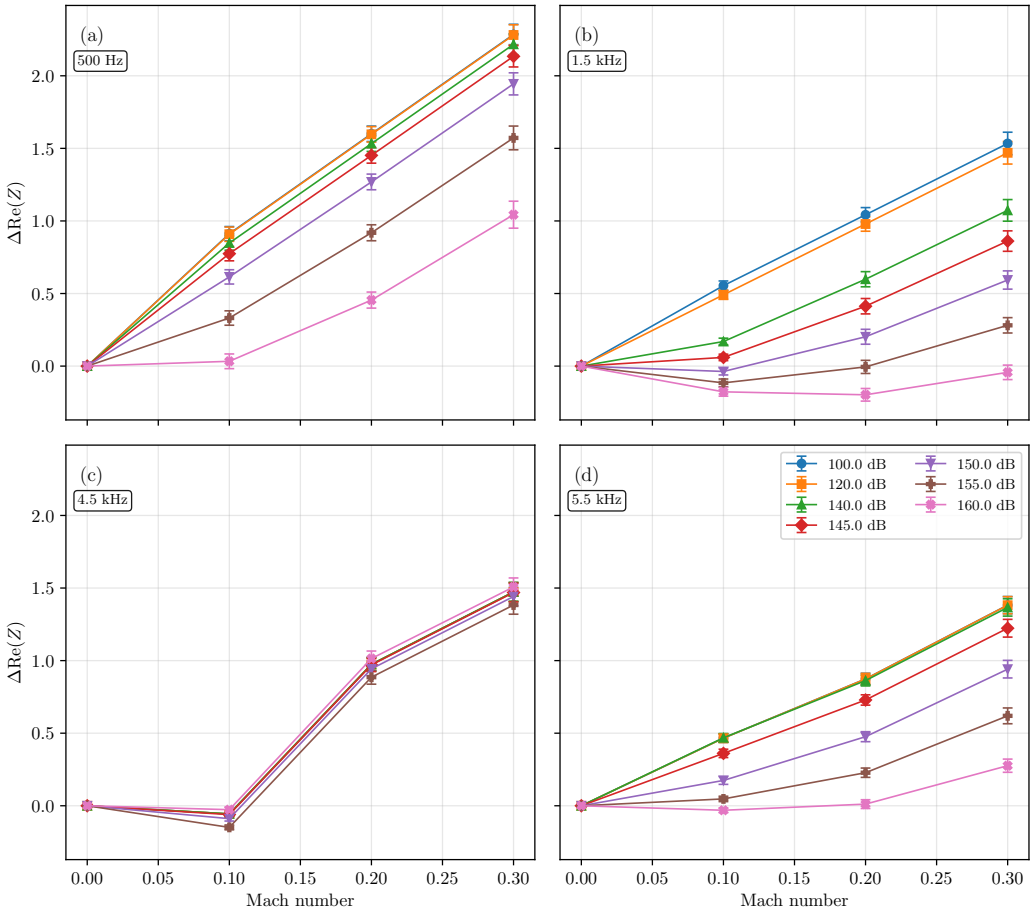

Fig. 10 Comparison of resistance against Mach, for different frequencies and total SPL.

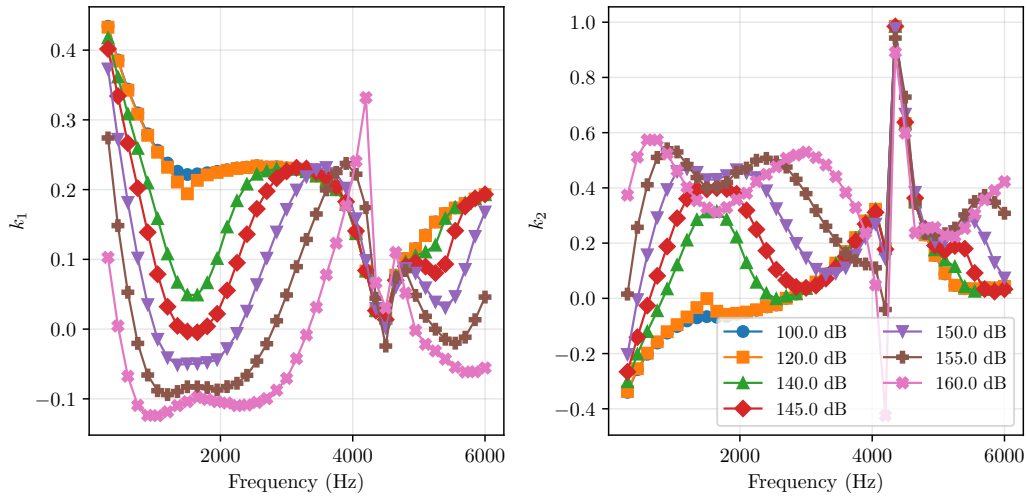

Fig. 11 Evolution of the k_1 and k_2 parameters as a function of frequency and SPL.

Declaration of Generative AI and AI-assisted technologies in the writing process

During the preparation of this work the authors used ChatGPT in order to improve readability. After using this tool, the authors reviewed and edited the content as needed and take full responsibility for the content of the publication.

Declaration of competing interest

The authors have no conflict of interest to declare.

Acknowledgments

R.R. is co-funded by the European Union (ERC, POROLEAF, 101103502). L.A. and F.A. are co-funded by the European Union ((ERC, LINING, 101075903). Views and opinions expressed are however those of the authors only and do not necessarily reflect those of the European Union or the European Research Council Executive Agency. Neither the European Union nor the granting authority can be held responsible for them. The authors are grateful to Nicolas Fasano and Laurent Burel for their help in setting up the LDV flow seeder and creating the liner sample, respectively.

References

[1] Ma, X., and Su, Z., "Development of acoustic liner in aero engine: a review," *Science China Technological Sciences*, Vol. 63, No. 12, 2020, pp. 2491–2504. https://doi.org/10.1007/s11431-019-1501-3.

[2] Bauer, A. B., "Impedance theory and measurements on porous acoustic liners," *Journal of Aircraft*, Vol. 14, No. 8, 1977, pp. 720–728. https://doi.org/10.2514/3.58844.

[3] Ingard, U., and Ising, H., "Acoustic nonlinearity of an orifice," *The journal of the Acoustical Society of America*, Vol. 42, No. 1, 1967, pp. 6–17. https://doi.org/10.1121/1.1910576.

[4] Melling, T. H., "The acoustic impendance of perforates at medium and high sound pressure levels," *Journal of Sound and Vibration*, Vol. 29, No. 1, 1973, pp. 1–65. https://doi.org/10.1016/S0022-460X(73)80125-7.

[5] Tam, C. K., Kurbatskii, K. A., Ahuja, K., and Gaeta Jr, R., "A numerical and experimental investigation of the dissipation mechanisms of resonant acoustic liners," *Journal of Sound and Vibration*, Vol. 245, No. 3, 2001, pp. 545–557. https://doi.org/10.1006/jsvi.2001.3571.

[6] Jing, X., and Sun, X., "Sound-excited flow and acoustic nonlinearity at an orifice," *Physics of Fluids*, Vol. 14, No. 1, 2002, pp. 268–276. https://doi.org/10.1063/1.1423934.

[7] Dean, P. D., "An in situ method of wall acoustic impedance measurement in flow ducts," *Journal of Sound and Vibration*, Vol. 34, No. 1, 1974, pp. 97–IN6. https://doi.org/10.1016/S0022-460X(74)80357-3.

[8] Bonomo, L. A., Quintino, N. T., Spillere, A. M., Murray, P. B., and Cordioli, J. A., "A comparison of in situ and impedance eduction experimental techniques for acoustic liners with grazing flow and high sound pressure level," *International Journal of Aeroacoustics*, Vol. 23, No. 1-2, 2024, pp. 60–83. https://doi.org/10.1177/1475472X231225629.

[9] Renou, Y., and Aurégan, Y., "Failure of the Ingard–Myers boundary condition for a lined duct: An experimental investigation," *The Journal of the Acoustical Society of America*, Vol. 130, No. 1, 2011, pp. 52–60. https://doi.org/10.1121/1.3586789.

[10] Roncen, R., Piot, E., Méry, F., Simon, F., Jones, M. G., and Nark, D. M., "Wavenumber-based impedance eduction with a shear grazing flow," *AIAA Journal*, Vol. 58, No. 7, 2020, pp. 3040–3050. https://doi.org/10.2514/1.J059100.

[11] Schulz, A., Weng, C., Bake, F., Enghardt, L., and Ronneberger, D., "Modeling of liner impedance with grazing shear flow using a new momentum transfer boundary condition," *23rd AIAA/CEAS aeroacoustics conference*, 2017, p. 3377. https://doi.org/10.2514/6.2017-3377.

[12] Weng, C., Schulz, A., Ronneberger, D., Enghardt, L., and Bake, F., "Flow and viscous effects on impedance eduction," *AIAA Journal*, Vol. 56, No. 3, 2018, pp. 1118–1132. https://doi.org/10.2514/1.J055838.

[13] Roncen, R., Méry, F., Piot, E., and Klotz, P., "Spatially-varying impedance model for locally reacting acoustic liners at a high sound intensity," *Journal of Sound and Vibration*, Vol. 524, 2022, p. 116741. https://doi.org/10.1016/j.jsv.2021.116741.

[14] Quintino, N. T., Bonomo, L. A., Cordioli, J. A., Jones, M. G., Howerton, B. M., Nark, D. M., and Avallone, F., "Comparison of impedance eduction test rigs with different boundary-layer profiles," *AIAA Journal*, Vol. 63, No. 11, 2025, pp. 4872–4883.

[15] Roncen, R., "Revisiting nonlinear impedance in acoustic liners," *Journal of Sound and Vibration*, Vol. 608, 2025, p. 119058. https://doi.org/10.1016/j.jsv.2025.119058.

[16] Roncen, R., and Cardesa, J., "Generic and broadband non-linear time domain impedance boundary condition," *Journal of Sound and Vibration*, 2023, p. 117691. https://doi.org/10.1016/j.jsv.2023.117691.

[17] Boden, H., Shah, S. A., and Boij, S., "Comparison of Experimental Data and Empirical Models for Nonlinear Acoustic Properties of Perforates," *30th AIAA/CEAS Aeroacoustics Conference (2024)*, 2024, p. 3137. https://doi.org/10.2514/6.2024-3137.

[18] Allard, J., and Atalla, N., *Propagation of Sound in Porous Media: Modelling Sound Absorbing Materials 2e*, John Wiley & Sons, New York, 2009. https://doi.org/10.1002/9780470747339.

[19] Atalla, N., and Sgard, F., "Modeling of perforated plates and screens using rigid frame porous models," *Journal of sound and vibration*, Vol. 303, No. 1-2, 2007, pp. 195–208. https://doi.org/10.1016/j.jsv.2007.01.012.

[20] Bruneau, M., *Fundamentals of acoustics*, London, UK, 2006.

[21] Guess, A., "Calculation of perforated plate liner parameters from specified acoustic resistance and reactance," *Journal of Sound and Vibration*, Vol. 40, No. 1, 1975, pp. 119–137. https://doi.org/10.1016/S0022-460X(75)80234-3.

[22] Cummings, A., "Transient and multiple frequency sound transmission through perforated plates at high amplitude," *The Journal of the Acoustical Society of America*, Vol. 79, No. 4, 1986, pp. 942–951. https://doi.org/10.1121/1.393691.

[23] Temiz, M. A., Tournadre, J., Arteaga, I. L., and Hirschberg, A., "Non-linear acoustic transfer impedance of micro-perforated plates with circular orifices," *Journal of Sound and Vibration*, Vol. 366, 2016, pp. 418–428. https://doi.org/10.1016/j.jsv.2015.12.022.

[24] Shah, S. A., Bodén, H., and Boij, S., "An experimental study on three-port measurements for acoustic characterisation of the perforate reactance," *Journal of Sound and Vibration*, 2024, p. 118776. https://doi.org/10.1016/j.jsv.2024.118776.

[25] Dean III, L., and Feder, E., "Analytical and experimental studies for predicting noise attenuation in acoustically treated ducts for turbofan engines," Tech. rep., NASA, 1969.

[26] Delorme, P., Mazet, P., Peyret, C., and Ventribout, Y., "Computational aeroacoustics applications based on a discontinuous Galerkin method," *Comptes Rendus Mécanique*, Vol. 333, No. 9, 2005, pp. 676–682. https://doi.org/10.1016/j.crme.2005.07.007.

[27] Ventribout, Y., "Contrôle des perturbations aéroacoustiques par impédances de parois: application à un modèle de matériaux poreux," Ph.D. thesis, Ecole nationale superieure de l'aeronautique et de l'espace, 2006.

[28] Monteghetti, F., "Analysis and discretization of time-domain impedance boundary conditions in aeroacoustics," Ph.D. thesis, Institut Supérieur de l'Aéronautique et de l'Espace (ISAE-SUPAERO . . . , 2018.

[29] Bonomo, L. A., Quintino, N. T., Cordioli, J. A., Avallone, F., Jones, M. G., Howerton, B. M., and Nark, D. M., "A comparison of impedance eduction test rigs with different flow profiles," *AIAA AVIATION 2023 Forum*, 2023, p. 3346. https://doi.org/10.2514/6.2023-3346.

[30] Jones, M. G., and Nark, D. M., "Partition Thickness Considerations for Additively Manufactured Acoustic Liners," 2023. URL https://ntrs.nasa.gov/citations/20230013028.

[31] Lafont, V., Méry, F., Roncen, R., Simon, F., and Piot, E., "Liner impedance eduction under shear grazing flow at a high sound pressure level," *AIAA Journal*, Vol. 58, No. 3, 2020, pp. 1107–1117. https://doi.org/10.2514/1.J058756.

[32] Paduano, A., Scarano, F., Cordioli, J., Casalino, D., and Avallone, F., "On the impact of the turbulent grazing flow development on the acoustic response of an acoustic liner," *arXiv preprint arXiv:2507.22714*, 2025.

[33] Léon, O., Méry, F., Piot, E., and Conte, C., "Near-wall aerodynamic response of an acoustic liner to harmonic excitation with grazing flow," *Experiments in fluids*, Vol. 60, No. 9, 2019, p. 144. https://doi.org/10.1007/s00348-019-2791-5.